VEMcomp: A MATLAB tool for semilinear parabolic PDEs in 2D and 3D

Massimo Frittelli, Anotida Madzvamuse, Ivonne Sgura

March 10, 2023

Abstract

We present a Virtual Element MATLAB solver for elliptic or parabolic, linear or semilinear PDEs in two or three space dimensions., which we call VEMcomp. The library covers PDEs posed on different geometries, such as bulk, surface, or bulk-surface PDE probems. The solver employs the Virtual Element Method of lowest polynomial order $k = 1$ on general polygonal or polyhedral meshes. VEMcomp has three purposes. First, for special geometries, VEMcomp generates polygonal and polyhedral meshes optimized for fast matrix assembly. Second, given a mesh for the considered geometry, possibly generated with an external program, VEMcomp computes all the matrices of the method. Third, for multiple classes of PDEs, surface and bulk-surface PDEs, VEMcomp solves the considered PDE problem with the Virtual Element method with a user-friendly interface. An extensive set of examples illustrates the usage of the library and the optimal convergence rate of the method.

1 Introduction

The Virtual Element Method (VEM) was first proposed in [8] for elliptic problems in two space dimensions as a generalization of the Finite Element Method, where the mesh elements can be general polygons instead of triangles. The usage of polygons with arbitrarily many edges is made possible by enriching the local space of polynomials with suitable non-polynomial functions defined as solutions of an element-wise problem. This elegant idea ensures the optimal polynomial accuracy of the method.

The immediate success of VEM is due to the multiple benefits of its geometric flexibility. Among such benefits, we mention: (i) efficient mesh refinement techniques [18, 38], (ii) numerical solutions with high global regularity [11, 13], (iii) accurate approximation of boundaries [15, 17, 20], (iv) easy mesh pasting [12, 27], and (v) easy handling of complex domain shapes and cuts [16, 19].

Motivated by its multiple benefits, the VEM was quickly extended to numerous PDE problems and applications. A non-exhaustive list of models for which VEMs are now available comprises (i) linear elliptic problems in two [8, 15] and three [10] space dimensions, (ii) semilinear elliptic problems in two or three space dimensions [39], (iii) linear heat equation in two [37] and three [40] space dimensions, (iv) semilinear parabolic equations [2] and reaction-diffusion systems [30], (v) elasticity [7, 28] and plasticity [4] problems, (vi) phase-field models [3, 5], (vii) fluid dynamics [1, 14], (viii) fracture models [16], and recently (ix) surface [6, 27] and bulk-surface [23, 24] PDEs. Over ten years of its existence, the VEM has established itself as a reliable technology with desirable properties. This has stimulated the development of the first open-source VEM libraries and codes. Here will will recall some of these libraries. The work in [35] presents a MATLAB implementation of the baseline VEM application: the lowest order VEM for the Poisson problem in 2D. For the same problem, a high order VEM code in MATLAB is then provided in [29]. An Abaqus-MATLAB VEM code for coupled thermo-elasticity problems in 2D is presented in [21]. VEM libraries for elasticity problems in 2D are available in MATLAB/Octave [33] and C++ [34]. All the mentioned libraries are dedicated to specific use cases or applications and are confined to the two space dimensional setting.

To the best of the authors' knowledge, there is no open-source VEM library so far for PDE problems in three space dimensions and/or of surface or bulk-surface type. In this work, we contribute to

the field of VEM open-source libraries. We propose a MATLAB library, which we call VEMcomp, for elliptic and parabolic PDE problems in 2D and 3D, including bulk, surface and bulk-surface PDE problems. VEMcomp has three purposes:

1. For special geometries, both in 2D and 3D, such as rectangles, ellipses, parallelepipeds and ellipsoids, the library generates polygonal and polyhedral meshes specifically optimized for fast matrix assembly, following [23, 24];

2. Given any polygonal or polyhedral mesh -not necessarily generated with VEMcomp itself-, the library generates all the matrices involved in the method (e.g. mass, stiffness). For polygonal mesh generation, it is worth recalling the MATLAB library `PolyMesher` [36];

3. For multiple classes of PDE problems, the library performs matrix assembly and provides a black-box interface that allows the user to set the problem parameters, and returns the VEM numerical solution. For time-dependent problems, the time discretization is carried out with the Implicit-Explicit (IMEX) Euler method, which is proven to be simple and effective in combination with FEMs and VEMs for surface [26, 25] and bulk-surface PDEs [23, 24].

The structure of the paper is as follows. In Section 2 we state the multiple model problems to be addressed in this work, thereby motivating the functionalities of VEMcomp. In Section 3 we illustrate the VEMcomp facility for polygonal and polyhedral mesh generation. Section 4 presents two classes of VEMcomp dedicated to the computation of local VEM matrices. In Section 5 we showcase VEMcomp's user-friendly solver for the model problems outlined in Section 2. Section 6 showcases several numerical examples that illustrate at once the usage of VEMcomp and the optimal convergence of the Virtual Element Method.

2   Overview

VEMcomp is an object-oriented VEM library written in MATLAB. Compared to other existing VEM libraries, VEMcomp aims to fill the gap for (i) PDE problems in three space dimensions and (ii) PDE problems on complex geometries, such as surface or bulk-surface PDEs. In the remainder of this section, let $\Omega \subset \mathbb{R}^d$, $d = 2, 3$, be a compact domain in the d-dimensional Euclidean space. The first class of PDE problems covered by VEMcomp comprises elliptic and parabolic, linear and semilinear, bulk-only PDE systems of $n \in \mathbb{N}$ equations, and is given by

$$\begin{cases} \left[\dfrac{\partial u_i}{\partial t}\right] - d_i^\Omega \Delta u_i = f_i(u_1, \ldots, u_n, \mathbf{x}, [t]), & \mathbf{x} \in \Omega \qquad i = 1, \ldots, n; \\ u_i = 0 \quad \text{or} \quad \dfrac{\partial u_i}{\partial \mathbf{n}} = 0, & \mathbf{x} \in \partial\Omega \qquad i = 1, \ldots, n, \end{cases} \tag{1}$$

where Δ denotes the Laplace operator in Ω, $d_1^\Omega, \ldots, d_n^\Omega > 0$ are diffusion coefficients $T > 0$ is the final time, $f_1, \ldots, f_n$ are smooth enough linear or nonlinear functions. In (1), the expressions between square brackets appear in the parabolic (time-dependent) case, but not in the elliptic (stationary) case. The general model (1) comprises several notable bulk-only PDE problems that were solved with VEM in the literature, such as (i) linear [8, 10, 15] and semilinear elliptic problems [39], (ii) linear [37] and semilinear parabolic problems [2] including reaction-diffusion systems [30]. If $\Gamma = \partial\Omega$ is a sufficiently smooth manifold, a second class of PDEs that fall in VEMcomp's domain is the following class of surface PDEs or systems of $m \in \mathbb{N}$ surface PDEs:

$$\left[\dfrac{\partial u_j}{\partial t}\right] - d_j^\Gamma \Delta_\Gamma u_j = g_j(u_1, \ldots, u_n, \mathbf{x}, [t]), \qquad \mathbf{x} \in \Gamma, \qquad j = 1, \ldots, m, \tag{2}$$

where Δ_Γ represents the Laplace operator on Γ, $d_1^\Gamma, \ldots, d_m^\Gamma > 0$ are diffusion coefficients, $g_1, \ldots, g_m$ are smooth enough linear or nonlinear functions, $T > 0$ is the final time. In (2), the expressions between square brackets appear only in the time-dependent case. The general model (2) encompasses several surface PDE (SPDE) models of interest, such as elliptic SPDEs [6, 27] and surface reaction-diffusion systems (SRDSs) [31, 32].

The third and most complex class of PDE problems addressed in this work is given by bulk-surface PDEs of the following form:

$$\begin{cases} \left[\dfrac{\partial u_i}{\partial t}\right] - d_i^\Omega \Delta u_i = f_i(u_1,\ldots,u_n,\mathbf{x},[t]), & \mathbf{x}\in\Omega, \qquad i=1,\ldots,n; \\[2mm] \left[\dfrac{\partial v_j}{\partial t}\right] - d_j^\Gamma \Delta_\Gamma v_j = g_j(u_1,\ldots,u_n,v_1,\ldots,v_m,\mathbf{x},[t]), & \mathbf{x}\in\Gamma, \qquad j=1,\ldots,m; \\[2mm] \dfrac{\partial u_i}{\partial \mathbf{n}} = h_i(u_1,\ldots,u_n,v_1,\ldots,v_m,\mathbf{x},[t]), & \mathbf{x}\in\Gamma, \qquad i=1,\ldots,n, \end{cases} \qquad (3)$$

where Δ and Δ_Γ represents the Laplace operator in Ω and the Laplace-Beltrami operator on Γ, $d_1^\Omega,\ldots,d_n^\Omega, d_1^\Gamma,\ldots,d_m^\Gamma > 0$ are diffusion coefficients, $f_1,\ldots,f_n, g_1,\ldots,g_m, h_1,\ldots,h_n$ are smooth enough linear or nonlinear functions, and $T > 0$ is the final time. In (3), the expressions between square brackets appear only in the time-dependent case. We recall that the VEM was extended to bulk-surface reaction-diffusion systems (BSRDSs) in two [23] and three [24] space dimensions, which fall within the general class (3).

In the next Sections we will illustrate in detail the three main facilities of VEMcomp: (i) polygonal and polyhedral mesh generation, (ii) computation of local VEM matrices, and (iii) matrix assembly and user-friendly solver for problems (1), (2), and (3).

3   Mesh generation and representation

Polygonal and polyhedral mesh generation is a niche topic, and very little software is available. For domains in two space dimensions, we mention PolyMesher [36]. To the best of the authors' knowledge, there is no open-source software for polyhedral mesh generation in three space dimensions. For special three dimensional domains, VEMcomp fills this gap. We point out that, when restricted to triangular (in 2D) or tetrahedral meshes (in 3D), the Virtual Element Method of low polynomial order $k = 1$ boils down to the Finite Element Method. This means that VEMcomp can be used as a FEM solver for surface and bulk-surface PDEs, when provided with triangular/tetrahedral meshes, for which countless open-source generators exist. We start by presenting basic classes that allow to represent single elements in two and three space dimensions.

3.1   The class `element2d_dummy`

The class `element2d_dummy` represent a polygonal element in 2D. It contains minimal information that uniquely identify the element. To create an element with `NVert` vertexes, use the following constructor

```
obj = element2d_dummy(P);
```

where `P` is a `NVert` $\times$ 3 array containing the coordinates of the vertexes, ordered clockwise or counterclockwise. The vertexes have three coordinates, because two-dimensional elements are also faces of three-dimensional elements. When an `element2d_dummy` is created, the following properties are set by the above constructor

```
properties (SetAccess = private)
        P(:,3) double % Coordinates of vertexes
        NVert(1,1) double % Number of vertexes
end
```

When needed, an `element2d_dummy` can be provided with optional information contained in the following optional properties:

```
properties (SetAccess = private)
        P_ind(:,1) double = []
        is_boundary(1,1) logical
        is_square(1,1) logical
end
```

defined as follows:

- If the `element2d_dummy` is part of a mesh, and the array `PP` of size `NMesh` × 3 contains the coordinates of all the nodes, then the property `P_ind` contains the indexes of the nodes `P` of the `element2d_dummy`, i.e. `PP(P_ind,:)  = P;`

- The logical `is_boundary` determines if the `element2d_dummy` is a face of a three-dimensional element lying on the boundary Γ of the bulk domain Ω. This information is necessary for the assembly of VEM matrices;

- The logical `is_square` determines if the `element2d_dummy` is a square (for which the local VEM matrices are known in closed form).

3.2 The class `element3d_dummy`

The class `element3d_dummy` represent a polyhedral element in 3D. It contains minimal information that uniquely identify the element. To create an element with `NVert` vertexes and `NFaces` faces, use the following constructor

```
obj = element3d_dummy(P,Faces)
```

where `P` is a `NVert` × 3 array containing the coordinates of the vertexes in any order and `Faces` is a `NFaces` × 1 array of `element2d_dummy`. When an `element3d_dummy` is created, the following properties are set by the above constructor

```
properties (SetAccess = private)
        P(:,3) double % Coordinates of vertexes
        Faces(:,1) element2d_dummy % Faces
end
```

When needed, an `element3d_dummy` can be provided, through the above constructor, with the following optional properties:

```
properties (SetAccess = private)
        Pind(:,1) double = []
        iscube(1,1) logical
end
```

defined as follows:

- If the `element3d_dummy` is part of a mesh, and the array `PP` of size `NMesh` × 3 contains the coordinates of all the nodes, then the property `P_ind` contains the indexes of the nodes `P` of the `element3d_dummy`, i.e. `PP(P_ind,:)  = P;`

- The logical `is_cube` determines if the `element3d_dummy` is a cube (for which the local VEM matrices are known in closed form).

3.3 Generating meshes for special geometries

4 Computation of local matrices

VEMcomp has two classes specifically designed for the computation of the local VEM matrices of lowest polynomial order $k = 1$ (stiffness, mass, and consistency matrices) in two and three space dimensions: `element2d` and `element3d`, respectively. VEMcomp relies on the following assumptions on the mesh:

- in 2D, every (polygonal) element is star-shaped w.r.t. at least one point.

- in 3D, every (polyhedral) element is star-shaped w.r.t. at least one point and so are all of its faces.

4.1 The class `element2d`

The class `element2d` represents a polygonal element in 2D with `NVert` vertexes that is star-shaped w.r.t. at least one point. To create an instance of the class, use the following constructor

```
obj = element2d(P, P0);
```

where

- `P` is a `NVert` $\times$ 3 matrix whose rows are the coordinates of the ordered vertexes.

- `P0`, of size 1×3, is a point w.r.t. which the element is star-shaped.

Upon initialisation, the object stores `P` and `P0` and automatically computes several other `properties` of the element:

```
properties(SetAccess = private)
        P(:,3) double
        P0(1,3) double
        NVert(1,1) double
        Area(1,1) double
        OrientedArea(1,3) double
        Centroid (1,3) double
        Diameter(1,1) double
        K(:,:) double
        M(:,:) double
end
```

that can be queried from the object. In the above:

- `NVert` is the number of vertexes

- `Area` is the surface area of the element

- `OrientedArea` is a vector orthogonal to the element whose modulus is the element area

- `Centroid` is the centroid of the element

- `Diameter` is the diameter of the element

- `K` is the local stiffness matrix

- `M` is the local mass matrix

The usage of `element2d` will be demonstrated later on.

4.2 The class `element3d`

The class `element3d` represents a polygonal element in 3D with `NVert` vertexes that is star-shaped w.r.t. at least one point and whose faces fulfill the same property. To create an instance of the class, use the following constructor

```
obj = element3d(Faces, P, P0);
```

where

- `Faces` is a `NFaces` $\times$ 1 array of `element2d` representing the faces

- `P` is a `NVert` $\times$ 3 matrix whose rows are the coordinates of the vertexes

- `P0` is a point w.r.t. which the element is star-shaped.

We remark that, even if the vertexes `P` are already contained in the `Faces`, the `property` `P` is still needed to specify vertex ordering. Upon initialisation, the object stores `Faces`, `P`, and `P0` and automatically computes several other public `properties` of the element:

```
properties(SetAccess = private)
        Faces(:,1) element2d
        P(:,3) double
        P0(1,3) double
        NVert(1,1) double
        NFaces(1,1) double
        Volume(1,1) double
        Centroid(1,3) double
        Diameter(1,1) double
        K(:,:) double
        M(:,:) double
end
```

that can be queried from the object. In the above:

- `NVert` is the number of vertexes and `NFaces` is the number of faces

- `Volume`, `Centroid` and `Diameter` are self-explanatory

- `K` is the local stiffness matrix and `M` is the local mass matrix.

The usage of `element3d` will be demonstrated later on.

4.3   A worked example in 2D: the unit square

Here we will show the usage of `element2d` to compute the local matrices of the unit square, thereby presenting the closed-form counterpart. Consider the unit square contained in the xy-plane:

$$F = \{(x, y, z) \in \mathbb{R}^3 | (x, y) \in [0, 1]^2, \ z = 0\}, \tag{4}$$

which can be thought of as the polygon enclosed by the vertexes $(0, 0, 0)$, $(0, 1, 0)$, $(1, 1, 0)$, and $(1, 0, 0)$. Notice that node ordering affects the resulting matrices. We start by computing the closed form of the VEM local mass and stiffness matrices of F for the lowest order case $k = 1$.

As shown in [9], the computation of the mass and stiffness matrices relies on three fundamental matrices:

- $B \in \mathbb{R}^{3 \times \texttt{NVert}}$;

- $D \in \mathbb{R}^{\texttt{NVert} \times 3}$;

- $H \in \mathbb{R}^{3 \times 3}$,

whose lengthy definitions we do not report here. With the above matrices in hand, the following matrices can be obtained:

- $G := BD \in \mathbb{R}^{3 \times 3}$;

- $\widetilde{G} := \begin{bmatrix} 0 & 0 & 0 \\ 0 & 1 & 0 \\ 0 & 0 & 1 \end{bmatrix} G \in \mathbb{R}^{3 \times 3}$;

- $\Pi_*^{\nabla} := G^{-1}B \in \mathbb{R}^{3 \times \texttt{NVert}}$;

- $\Pi^{\nabla} := D\Pi_*^{\nabla} \in \mathbb{R}^{\texttt{NVert} \times \texttt{NVert}}$.

Finally, the local stiffness and mass matrices are given by

$$K = (\Pi_*^{\nabla})^T \widetilde{G} \Pi_*^{\nabla} + (I - \Pi^{\nabla})^T (I - \Pi^{\nabla}); \tag{5}$$

$$M = (\Pi_*^{\nabla})^T H \Pi_*^{\nabla} + \text{Area(F)}(I - \Pi^{\nabla})^T (I - \Pi^{\nabla}). \tag{6}$$

For the unit square F, as shown in [9], it holds that

$$B = \frac{1}{4} \begin{bmatrix} 1 & 1 & 1 & 1 \\ -\sqrt{2} & \sqrt{2} & \sqrt{2} & -\sqrt{2} \\ -\sqrt{2} & -\sqrt{2} & \sqrt{2} & \sqrt{2} \end{bmatrix}; \tag{7}$$

$$D = \frac{1}{4} \begin{bmatrix} 4 & -\sqrt{2} & -\sqrt{2} \\ 4 & \sqrt{2} & -\sqrt{2} \\ 4 & \sqrt{2} & \sqrt{2} \\ 4 & -\sqrt{2} & \sqrt{2} \end{bmatrix}; \tag{8}$$

$$H = \frac{1}{24} \begin{bmatrix} 24 & 0 & 0 \\ 0 & 1 & 0 \\ 0 & 0 & 1 \end{bmatrix}. \tag{9}$$

It follows that

$$G = \frac{1}{2} \begin{bmatrix} 2 & 0 & 0 \\ 0 & 1 & 0 \\ 0 & 0 & 1 \end{bmatrix}, \qquad \widetilde{G} = \frac{1}{2} \begin{bmatrix} 0 & 0 & 0 \\ 0 & 1 & 0 \\ 0 & 0 & 1 \end{bmatrix}; \tag{10}$$

$$\Pi_*^\nabla = \frac{1}{4} \begin{bmatrix} 1 & 1 & 1 & 1 \\ -2\sqrt{2} & 2\sqrt{2} & 2\sqrt{2} & -2\sqrt{2} \\ -2\sqrt{2} & -2\sqrt{2} & 2\sqrt{2} & 2\sqrt{2} \end{bmatrix}; \tag{11}$$

$$\Pi^\nabla = \frac{1}{4} \begin{bmatrix} 3 & 1 & -1 & 1 \\ 1 & 3 & 1 & -1 \\ -1 & 1 & 3 & 1 \\ 1 & -1 & 1 & 3 \end{bmatrix}. \tag{12}$$

We finally obtain the local stiffness and mass matrices:

$$K = \frac{1}{4} \begin{bmatrix} 3 & -1 & -1 & -1 \\ -1 & 3 & -1 & -1 \\ -1 & -1 & 3 & -1 \\ -1 & -1 & -1 & 3 \end{bmatrix}; \tag{13}$$

$$M = \frac{1}{48} \begin{bmatrix} 17 & -9 & 13 & -9 \\ -9 & 17 & -9 & 13 \\ 13 & -9 & 17 & -9 \\ -9 & 13 & -9 & 17 \end{bmatrix}. \tag{14}$$

We now show the usage of `element2d` to compute the matrices K and M numerically. To this end, we need to create an object of class `element2d`. To call the constructor, we define the array P

```
P = [0 0 0; 0 1 0; 1 1 0; 1 0 0];
```

containing the vertexes of F and the array P0 as

```
P0 = [.5 .5 0];
```

because F is star-shaped w.r.t. P0. Notice that, since F is convex, P0 can be chosen as any point in F, even a vertex. We are ready to create the object:

```
F = element2d(P, P0)
```

Because there is no semicolon in the above command, the following output appears in the command window:

```
E1 =

  element2d with properties:

            P: [4x3 double]
```

```
              P0: [0.5000 0.5000 0]
           NVert: 4
            Area: 1
    OrientedArea: [0 0 -1]
        Centroid: [0.5000 0.5000 0]
        Diameter: 1.4142
               K: [4x4 double]
               M: [4x4 double]
```

Accidentally, the `Centroid` coincides with `P0`. By querying the stiffness and mass matrices of `F` (with `format rat` for better readability), we can see the outputs

```
>> E1.K

ans =

        3/4           -1/4           -1/4           -1/4
       -1/4            3/4           -1/4           -1/4
       -1/4           -1/4            3/4           -1/4
       -1/4           -1/4           -1/4            3/4

>> E1.M

ans =

      17/48           -3/16          13/48           -3/16
      -3/16           17/48          -3/16          13/48
      13/48           -3/16          17/48           -3/16
      -3/16           13/48          -3/16          17/48
```

which agree with (13)-(14).

4.4 A worked example in 3D: the unit cube

Here we will show the usage of `element3d` to compute the local matrices of the unit cube $E = [0,1]^3$, thereby presenting the closed-form counterpart. Because vertex ordering is reflected in the resulting matrices, we order the vertexes as follows:

$$(0,0,0)\ (0,0,1)\ (0,1,0)\ (0,1,1)\ (1,0,0)\ (1,0,1)\ (1,1,0)\ (1,1,1). \tag{15}$$

We start by computing the closed form of the VEM local mass and stiffness matrices of E for the lowest order case $k = 1$. As shown in [9], the computation of the mass and stiffness matrices relies on three fundamental matrices, similarly to the 2D case:

- $B \in \mathbb{R}^{4 \times \texttt{NVert}}$;

- $D \in \mathbb{R}^{\texttt{NVert} \times 4}$;

- $H \in \mathbb{R}^{4 \times 4}$,

whose lengthy definitions we do not report here. With the above matrices in hand, the following matrices can be obtained:

- $G := BD \in \mathbb{R}^{4 \times 4}$;

- $\widetilde{G} := \begin{bmatrix} 0 & 0 & 0 & 0 \\ 0 & 1 & 0 & 0 \\ 0 & 0 & 1 & 0 \\ 0 & 0 & 0 & 1 \end{bmatrix} G \in \mathbb{R}^{4 \times 4}$;

- $\Pi_*^{\nabla} := G^{-1} B \in \mathbb{R}^{4 \times \texttt{NVert}}$;

- $\Pi^\nabla := D\Pi_*^\nabla \in \mathbb{R}^{\mathrm{NVert}\times\mathrm{NVert}}$.

Finally, the local stiffness and mass matrices are given by

$$K = (\Pi_*^\nabla)^T \widetilde{G}\Pi_*^\nabla + \mathrm{Diam}(E)(I - \Pi^\nabla)^T(I - \Pi^\nabla); \tag{16}$$

$$M = (\Pi_*^\nabla)^T H\Pi_*^\nabla + \mathrm{Volume}(\mathrm{F})(I - \Pi^\nabla)^T(I - \Pi^\nabla). \tag{17}$$

For the unit cube E, it is possible to show that

$$B = \frac{1}{8\sqrt{3}}\begin{bmatrix} \sqrt{3} & \sqrt{3} & \sqrt{3} & \sqrt{3} & \sqrt{3} & \sqrt{3} & \sqrt{3} & \sqrt{3} \\ -2 & -2 & -2 & -2 & 2 & 2 & 2 & 2 \\ -2 & -2 & 2 & 2 & -2 & -2 & 2 & 2 \\ -2 & 2 & -2 & 2 & -2 & 2 & -2 & 2 \end{bmatrix}; \tag{18}$$

$$D = \frac{1}{2\sqrt{3}}\begin{bmatrix} 2\sqrt{3} & -1 & -1 & -1 \\ 2\sqrt{3} & -1 & -1 & 1 \\ 2\sqrt{3} & -1 & 1 & -1 \\ 2\sqrt{3} & -1 & 1 & 1 \\ 2\sqrt{3} & 1 & -1 & -1 \\ 2\sqrt{3} & 1 & -1 & 1 \\ 2\sqrt{3} & 1 & 1 & -1 \\ 2\sqrt{3} & 1 & 1 & 1 \end{bmatrix}; \tag{19}$$

$$H = \frac{1}{36}\begin{bmatrix} 36 & 0 & 0 & 0 \\ 0 & 1 & 0 & 0 \\ 0 & 0 & 1 & 0 \\ 0 & 0 & 0 & 1 \end{bmatrix}. \tag{20}$$

It follows that

$$G = \frac{1}{3}\begin{bmatrix} 3 & 0 & 0 & 1 \\ 0 & 1 & 0 & 0 \\ 0 & 0 & 1 & 0 \\ 0 & 0 & 0 & 1 \end{bmatrix}, \qquad \widetilde{G} = \frac{1}{3}\begin{bmatrix} 0 & 0 & 0 & 1 \\ 0 & 1 & 0 & 0 \\ 0 & 0 & 1 & 0 \\ 0 & 0 & 0 & 1 \end{bmatrix}; \tag{21}$$

$$\Pi_*^\nabla = \frac{1}{8}\begin{bmatrix} 1 & 1 & 1 & 1 & 1 & 1 & 1 & 1 \\ -2\sqrt{3} & -2\sqrt{3} & -2\sqrt{3} & -2\sqrt{3} & 2\sqrt{3} & 2\sqrt{3} & 2\sqrt{3} & 2\sqrt{3} \\ -2\sqrt{3} & -2\sqrt{3} & 2\sqrt{3} & 2\sqrt{3} & -2\sqrt{3} & -2\sqrt{3} & 2\sqrt{3} & 2\sqrt{3} \\ -2\sqrt{3} & 2\sqrt{3} & -2\sqrt{3} & 2\sqrt{3} & -2\sqrt{3} & 2\sqrt{3} & -2\sqrt{3} & 2\sqrt{3} \end{bmatrix}; \tag{22}$$

$$\Pi^\nabla = \frac{1}{4}\begin{bmatrix} 2 & 1 & 1 & 0 & 1 & 0 & 0 & -1 \\ 1 & 2 & 0 & 1 & 0 & 1 & -1 & 0 \\ 1 & 0 & 2 & 1 & 0 & -1 & 1 & 0 \\ 0 & 1 & 1 & 2 & -1 & 0 & 0 & 1 \\ 1 & 0 & 0 & -1 & 2 & 1 & 1 & 0 \\ 0 & 1 & -1 & 0 & 1 & 2 & 0 & 1 \\ 0 & -1 & 1 & 0 & 1 & 0 & 2 & 1 \\ -1 & 0 & 0 & 1 & 0 & 1 & 1 & 2 \end{bmatrix}. \tag{23}$$

We finally obtain the local stiffness and mass matrices:

$$
K = \frac{1}{16}
\begin{bmatrix}
3 & 1 & 1 & -1 & 1 & -1 & -1 & -3 \\
1 & 3 & -1 & 1 & -1 & 1 & -3 & -1 \\
1 & -1 & 3 & 1 & -1 & -3 & 1 & -1 \\
-1 & 1 & 1 & 3 & -3 & -1 & -1 & 1 \\
1 & -1 & -1 & -3 & 3 & 1 & 1 & -1 \\
-1 & 1 & -3 & -1 & 1 & 3 & -1 & 1 \\
-1 & -3 & 1 & -1 & 1 & -1 & 3 & 1 \\
-3 & -1 & -1 & 1 & -1 & 1 & 1 & 3
\end{bmatrix}
$$

$$
+ \frac{\sqrt{3}}{4}
\begin{bmatrix}
2 & -1 & -1 & 0 & -1 & 0 & 0 & 1 \\
-1 & 2 & 0 & -1 & 0 & -1 & 1 & 0 \\
-1 & 0 & 2 & -1 & 0 & 1 & -1 & 0 \\
0 & -1 & -1 & 2 & 1 & 0 & 0 & -1 \\
-1 & 0 & 0 & 1 & 2 & -1 & -1 & 0 \\
0 & -1 & 1 & 0 & -1 & 2 & 0 & -1 \\
0 & 1 & -1 & 0 & -1 & 0 & 2 & -1 \\
1 & 0 & 0 & -1 & 0 & -1 & -1 & 2
\end{bmatrix} ;
$$

$$(24)$$

$$
M = \frac{1}{96}
\begin{bmatrix}
51 & -22 & -22 & 1 & -22 & 1 & 1 & 24 \\
-22 & 51 & 1 & -22 & 1 & -22 & 24 & 1 \\
-22 & 1 & 51 & -22 & 1 & 24 & -22 & 1 \\
1 & -22 & -22 & 51 & 24 & 1 & 1 & -22 \\
-22 & 1 & 1 & 24 & 51 & -22 & -22 & 1 \\
1 & -22 & 24 & 1 & -22 & 51 & 1 & -22 \\
1 & 24 & -22 & 1 & -22 & 1 & 51 & -22 \\
24 & 1 & 1 & -22 & 1 & -22 & -22 & 51
\end{bmatrix} .
$$

$$(25)$$

We now show the usage of `element3d` to compute the matrices K and M numerically. To this end, we need to create an object of class `element3d`. To call the constructor, we first need to create six instances of `element2d` representing the faces of E:

```
P1 = [0 0 0; 0 1 0; 1 1 0; 1 0 0]; % bottom face
E1 = element2d(P1, sum(P1,1)/4);

P2 = [0 0 1; 0 1 1; 1 1 1; 1 0 1]; % top face
E2 = element2d(P2, sum(P2,1)/4);

P3 = [0 0 0; 0 1 0; 0 1 1; 0 0 1]; % back face
E3 = element2d(P3, sum(P3,1)/4);

P4 = [1 0 0; 1 1 0; 1 1 1; 1 0 1]; % front face
E4 = element2d(P4, sum(P4,1)/4);

P5 = [0 0 0; 1 0 0; 1 0 1; 0 0 1]; % left face
E5 = element2d(P5, sum(P5,1)/4);

P6 = [0 1 0; 1 1 0; 1 1 1; 0 1 1]; % right face
E6 = element2d(P6, sum(P6,1)/4);
```

For each of the faces, we have chosen P0 as the midpoint of its vertexes for convenience, but of course other choices are possible since every face is convex and thus star-shaped w.r.t. every point of the face itself. We are ready to create the `element3d`:

```
P = unique([P1; P2; P3; P4; P5; P6],'rows');
E = element3d([E1;E2;E3;E4;E5;E6], P, sum(P,1)/8);
```

We have used the command `unique` to extract a set of all vertexes with no repetitions. MATLAB will sort the vertexes in `P` in "increasing order", that is as in (15). Again, the `P0` is chosen as the midpoint of all vertexes for convenience. Let us have a look at the 3D element `E`:

```
>> E

E =

  element3d with properties:

        Faces: [6x1 element2d]
            P: [8x3 double]
           P0: [0.5000 0.5000 0.5000]
        NVert: 8
       NFaces: 6
       Volume: 1.0000
     Centroid: [0.5000 0.5000 0.5000]
     Diameter: 1.7321
            K: [8x8 double]
            M: [8x8 double]
```

By querying the stiffness and mass matrices of `E`, we can see the outputs

```
>> E.K

ans =

    1.0535   -0.3705   -0.3705   -0.0625   -0.3705   -0.0625   -0.0625    0.2455
   -0.3705    1.0535   -0.0625   -0.3705   -0.0625   -0.3705    0.2455   -0.0625
   -0.3705   -0.0625    1.0535   -0.3705   -0.0625    0.2455   -0.3705   -0.0625
   -0.0625   -0.3705   -0.3705    1.0535    0.2455   -0.0625   -0.0625   -0.3705
   -0.3705   -0.0625   -0.0625    0.2455    1.0535   -0.3705   -0.3705   -0.0625
   -0.0625   -0.3705    0.2455   -0.0625   -0.3705    1.0535   -0.0625   -0.3705
   -0.0625    0.2455   -0.3705   -0.0625   -0.3705   -0.0625    1.0535   -0.3705
    0.2455   -0.0625   -0.0625   -0.3705   -0.0625   -0.3705   -0.3705    1.0535
```

```
>> E.M

ans =

    17/32   -11/48   -11/48     1/96   -11/48     1/96     1/96      1/4
   -11/48    17/32     1/96   -11/48     1/96   -11/48      1/4     1/96
   -11/48     1/96    17/32   -11/48     1/96      1/4   -11/48     1/96
     1/96   -11/48   -11/48    17/32      1/4     1/96     1/96   -11/48
   -11/48     1/96     1/96      1/4    17/32   -11/48   -11/48     1/96
     1/96   -11/48      1/4     1/96   -11/48    17/32     1/96   -11/48
     1/96      1/4   -11/48     1/96   -11/48     1/96    17/32   -11/48
      1/4     1/96     1/96   -11/48     1/96   -11/48   -11/48    17/32
```

which agree with (24)-(25) up to machine precision.

5   Matrix assembly and user-friendly solver

[TO WRITE]

6 Numerical examples

We now present an extensive list of numerical experiments carried out in VEMcomp. The experiments showcase at once the usage of VEMcomp and the optimal convergence of the Virtual Element Method in its various forms.

6.1 Bulk-only problems

This first set of examples showcases the application of VEMcomp to bulk-only PDE problems of increasing complexity. In Example 6.1.1 we consider a Poisson problem on a two-dimensional domain. Examples 6.1.2 and 6.1.3 show the solution of a Poisson problem in three space dimensions on a cube and on a sphere, respectively.

6.1.1 Poisson problem on two-dimensional domain

[TODO]

6.1.2 Poisson equation on the cube

We now test the convergence of Virtual Elements, implemented via VEMcomp, for the following Poisson equation on the unit cube $\Omega = [0,1]^3$:

$$\begin{cases} - \quad \Delta u + u = (3\pi^2 + 1)\cos(\pi x)\cos(\pi y)\cos(\pi z) \qquad \text{in } \Omega \\ \quad \nabla u \cdot \boldsymbol{n} = 0 \qquad \text{on } \partial\Omega \end{cases} \tag{26}$$

whose exact solution is given by

$$u(x,y,z) = \cos(\pi x)\cos(\pi y)\cos(\pi z). \tag{27}$$

We consider a sequence of nine cubic meshes $i = 1,\ldots,9$. The i-th mesh, obtained by subdividing each dimension into $5i$ intervals, has $(5i)^3$ elements, $N_i = (5i + 1)^3$ nodes and meshsize $h_i = \sqrt{3}/(5i)$, as displayed in Table 1. On each mesh we solve the discrete problem, we compute the error in $L^2(\Omega)$ norm and the respective convergence rate. As shown in Table 1, the convergence in $L^2(\Omega)$ norm is optimal, i.e. quadratic. The numerical solution obtained on the finest mesh is plotted in Fig. 1.

Table 1: Poisson equation (26) on the unit cube $\Omega = [0,1]^3$. The VEM implemented in VEMcomp shows optimal quadratic convergence in $L^2(\Omega)$ norm.

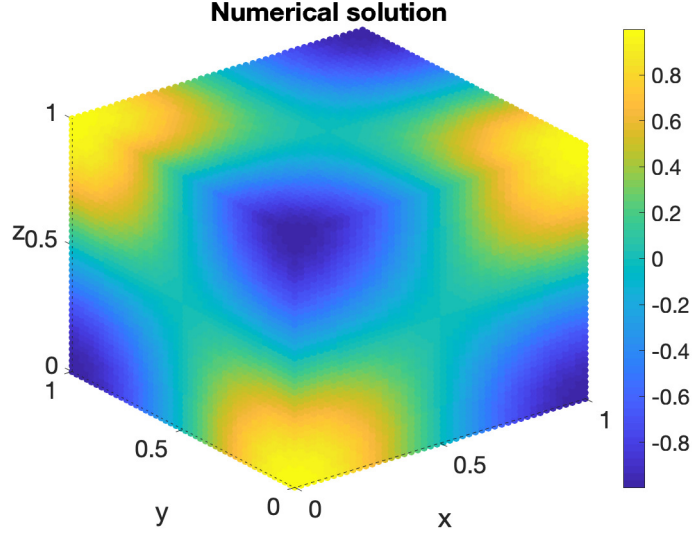| i	N	h	$L^2(\Omega)$ error	$L^2(\Omega)$ rate
1	216	0.3464	2.1663e-02	-
2	1331	0.1732	1.9934e-02	0.1200
3	4096	0.1155	1.0393e-02	1.6062
4	9261	0.0866	6.1700e-03	1.8126
5	17576	0.0693	4.0474e-03	1.8895
6	29791	0.0577	2.8484e-03	1.9269
7	46656	0.0495	2.1095e-03	1.9480
8	68921	0.0433	1.6235e-03	1.9611
9	97336	0.0385	1.2873e-03	1.9698

Figure 1: Poisson equation (26) on the unit cube $\Omega = [0,1]^3$: numerical solution obtained on the finest mesh for $i = 9$ with $N = 97336$ nodes.

6.1.3 Poisson equation on the sphere

We now consider another domain, the unit sphere Ω in 3D. The test problem, in spherical coordinates, is as follows

$$\begin{cases} - & \Delta u + u = 4(3 - 5r^2) + (1 - r^2)^2 \qquad \text{in } \Omega \\ & \nabla u \cdot \boldsymbol{n} = 0 \qquad \text{on } \partial\Omega \end{cases} \tag{28}$$

whose exact solution in spherical coordinates is given by

$$u(x, y, z) = (1 - r^2)^2 \tag{29}$$

We consider a sequence of four cubic meshes $i = 1, \ldots, 4$. The i-th mesh is obtained by subdividing each dimension into $5i$ intervals, thereby producing a cubic bounding mesh. The cubic elements that are not fully contained in the sphere are then discarded. Finally, the outer faces of the resulting cubic mesh are extruded to fill the outer part of the sphere with irregular 8-vertex polyhedra. Such a mesh is shown in Fig. 2. On each mesh we solve the discrete problem, we compute the error in $L^2(\Omega)$ norm and the respective convergence rate. As shown in Table 2, the convergence in $L^2(\Omega)$ norm is optimal, i.e. quadratic. The numerical solution obtained on the finest mesh is plotted in Fig. 3.
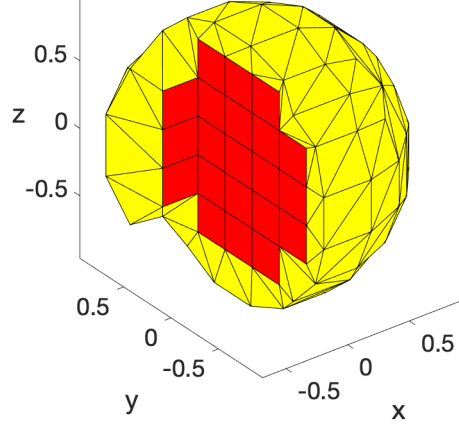
13

Extruded cubic mesh on the sphere

Figure 2: Example of an extruded cubic mesh on the unit sphere. The outermost elements, highlighted in yellow are irregular (but still star-shaped or even convex) 8-vertex polyhedra. The interior is filled with cubes (red).

Table 2: Poisson equation (28) on the unit sphere Ω in 3D. The VEM implemented in VEMcomp shows optimal quadratic convergence in $L^2(\Omega)$ norm.

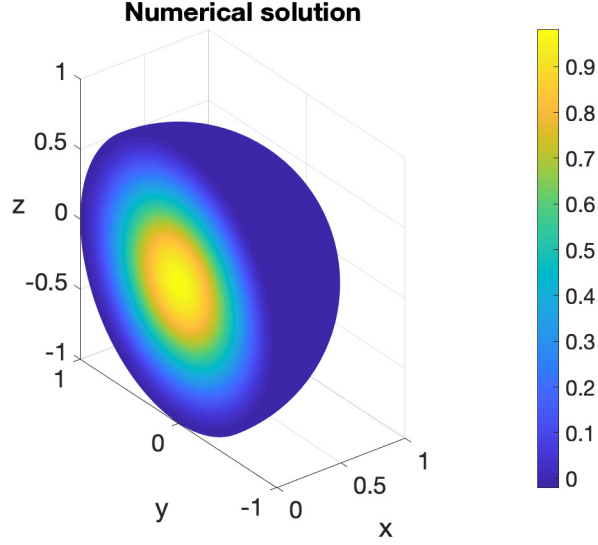| i	N	h	$L^2(\Omega)$ error	$L^2(\Omega)$ rate
1	111	0.6928	1.3767	-
2	799	0.3464	4.4137e-01	1.6412
3	5749	0.1732	1.2532e-01	1.8164
4	40381	0.0866	3.3139e-02	1.9190

Numerical solution

Figure 3: Poisson equation (28) on the unit sphere Ω in 3D: numerical solution obtained on the finest mesh for $i = 4$ with $N = 40381$ nodes.

6.2 Numerical examples for bulk-surface problems

We now apply VEMcomp to different types of BSPDEs. In Example 6.2.1 we show a baseline problem given by a bulk-surface linear elliptic problem on the sphere. Example 6.2.2 introduces the time variable, by addressing the bulk-surface linear heat equation on the sphere. In Example 6.2.3, we use VEMcomp to solve the top-end PDE problem considered in this work: a bulk-surface reaction-diffusion system (BSRDS) on the sphere.

6.2.1 Elliptic bulk-surface problem on the sphere

We numerically solve the following elliptic bulk-surface problem, found in [22], on the unit sphere Ω in 3D:

$$
\begin{cases}
- & \Delta u + u = xyz & \text{in } \Omega \\
- & \Delta_\Gamma v + v + \nabla u \cdot \boldsymbol{n} = 29xyz & \text{on } \partial\Omega \\
& \nabla u \cdot \boldsymbol{n} = -u + 2v & \text{on } \partial\Omega
\end{cases}
\tag{30}
$$

whose exact solution is given by

$$
\begin{aligned}
u(x, y, z) &= xyz, & (x, y, z) \in \Omega; \\
v(x, y, z) &= 2xyz, & (x, y, z) \in \partial\Omega.
\end{aligned}
$$

We consider the same sequence of four meshes Ω_i, $i = 1, 2, 3, 4$ of Experiment 6.1.3. The surface meshes are induced by the corresponding bulk mesh, i.e. $\Gamma_i = \partial\Omega_i$, $i = 1, \ldots, 4$. On each mesh we solve the discrete problem, we compute the error in $L^2(\Omega) \times L^2(\Gamma)$ norm and the respective convergence rate. As shown in Table 3, the convergence in $L^2(\Omega) \times L^2(\Gamma)$ norm is optimal, i.e. quadratic. The numerical solution obtained on the finest mesh is plotted in Fig. 4.

Table 3: Elliptic bulk-surface problem (30) on the unit sphere Ω in 3D. The VEM implemented in VEMcomp shows optimal quadratic convergence in $L^2(\Omega) \times L^2(\Gamma)$ norm. Times required for the solution of the linear system are shown.

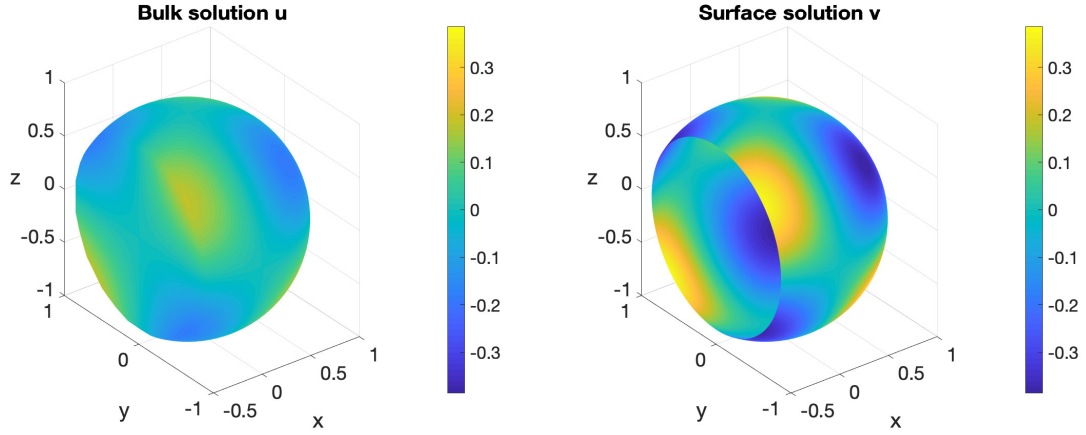| i	N	h	$L^2(\Omega) \times L^2(\Gamma)$ error	$L^2(\Omega) \times L^2(\Gamma)$ rate	Time (s)
1	111	0.6928	2.1985e-01	-	0.002159
2	799	0.3464	3.8387e-02	2.5178	0.015645
3	5749	0.1732	8.5674e-03	2.1637	0.197641
4	40381	0.0866	1.9884e-03	2.1072	5.994934

Figure 4: Elliptic bulk-surface problem (30) on the unit sphere Ω in 3D: numerical solution obtained on the finest mesh for $i = 4$ with $N = 40381$ nodes. Left: bulk component u. Right: surface component v.

6.2.2   Parabolic bulk-surface problem on the sphere

We numerically solve the following parabolic bulk-surface problem, found in [23], on the unit sphere Ω in 3D:

$$\begin{cases} \dot{u} - \Delta u = xyze^t & \text{in } \Omega \times [0, T]; \\ \dot{v} - \Delta_\Gamma v + \nabla u \cdot \boldsymbol{n} = 16xyze^t & \text{on } \partial\Omega \times [0, T]; \\ \nabla u \cdot \boldsymbol{n} = 3xyze^t & \text{on } \partial\Omega \times [0, T], \end{cases} \tag{31}$$

for final time $T = 1$, whose exact solution is given by

$$u(x, y, z, t) = xyze^t, \qquad (x, y, z, t) \in \Omega \times [0, T];$$
$$v(x, y, z, t) = 2xyze^t, \qquad (x, y, z, t) \in \partial\Omega \times [0, T].$$

We consider the same sequence of four meshes Ω_i, $i = 1, 2, 3, 4$ of Experiment 6.2.1. Correspondingly, we choose timesteps $\tau_i = 2^{1-i}$, $i = 1, 2, 3, 4$. On each mesh we solve the discrete problem, we compute the error in $L^2(\Omega) \times L^2(\Gamma)$ norm at the final time $T = 1$ and the respective convergence rate. As shown in Table 4, the convergence in $L^2(\Omega) \times L^2(\Gamma)$ norm is optimal, i.e. quadratic in space and linear in time. The numerical solution at the final time obtained on the finest mesh is plotted in Fig. 5.

16

Table 4: Parabolic bulk-surface problem (31) on the unit sphere Ω in 3D. The VEM implemented in VEMcomp shows optimal quadratic convergence in $L^2(\Omega) \times L^2(\Gamma)$ norm. Times required for the time integration are shown.

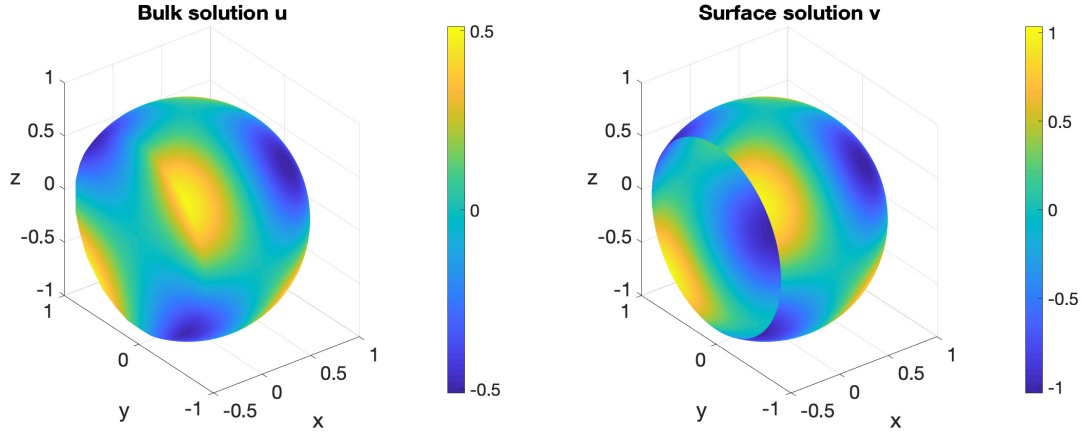| i	N	h	τ	$L^2(\Omega) \times L^2(\Gamma)$ error	$L^2(\Omega) \times L^2(\Gamma)$ rate	Time (s)
1	111	0.6928	1	1.2074	-	0.002417
2	799	0.3464	2.5e-1	4.3481e-01	1.4734	0.038881
3	5749	0.1732	6.25e-2	1.2110e-01	1.8442	2.134601
4	40381	0.0866	1.5625e-2	3.0881e-02	1.9714	287.345570

Figure 5: Parabolic bulk-surface problem (31) on the unit sphere Ω in 3D: numerical solution obtained on the finest mesh for $i = 4$ with $N = 40381$ nodes and timestep $\tau = 1.5625e - 2$. Left: bulk component u. Right: surface component v.

6.2.3 Bulk-surface reaction-diffusion system on the sphere

In this final example we solve the following BSRDS considered in [24].

References

[1] D Adak, D Mora, S Natarajan, and A Silgado. A virtual element discretization for the time dependent Navier–Stokes equations in stream-function formulation. *ESAIM: Mathematical Modelling and Numerical Analysis*, 55(5):2535–2566, 2021. `doi:10.1051/m2an/2021058`.

[2] D Adak, E Natarajan, and S Kumar. Convergence analysis of virtual element methods for semilinear parabolic problems on polygonal meshes. *Numerical Methods for Partial Differential Equations*, 35(1):222–245, 2019. `doi:10.1002/num.22298`.

[3] F Aldakheel, B Hudobivnik, A Hussein, and P Wriggers. Phase-field modeling of brittle fracture using an efficient virtual element scheme. *Computer Methods in Applied Mechanics and Engineering*, 341:443–466, 2018. `doi:10.1016/j.cma.2018.07.008`.

[4] F Aldakheel, B Hudobivnik, and P Wriggers. Virtual elements for finite thermo-plasticity problems. *Computational Mechanics*, 64:1347–1360, 2019. `doi:10.1007/s00466-019-01714-2`.

[5] P F Antonietti, L Beirão Da Veiga, S Scacchi, and M Verani. A $\mathcal{C}^1$ virtual element method for the Cahn–Hilliard equation with polygonal meshes. *SIAM Journal on Numerical Analysis*, 54(1):34–56, 2016. `doi:10.1137/15M1008117`.

[6] E Bachini, G Manzini, and M Putti. Arbitrary-order intrinsic virtual element method for elliptic equations on surfaces. *Calcolo*, 58(3):30, 2021. `doi:10.1007/s10092-021-00418-5`.

[7] L Beirão Da Veiga, F Brezzi, and L D Marini. Virtual elements for linear elasticity problems. *SIAM Journal on Numerical Analysis*, 51(2):794–812, 2013. `doi:10.1137/120874746`.

[8] L Beirão da Veiga, F Brezzi, A Cangiani, G Manzini, L D Marini, and A Russo. Basic principles of virtual element methods. *Mathematical Models and Methods in Applied Sciences*, 23(01):199–214, 2013. `doi:10.1051/m2an/2013138`.

[9] L Beirão da Veiga, F Brezzi, L D Marini, and A Russo. The hitchhiker's guide to the virtual element method. *Mathematical models and methods in applied sciences*, 24(08):1541–1573, 2014. `doi:10.1142/S021820251440003X`.

[10] L Beirão Da Veiga, F Dassi, and A Russo. High-order virtual element method on polyhedral meshes. *Computers & Mathematics with Applications*, 74(5):1110–1122, 2017. `doi:10.1016/j.camwa.2017.03.021`.

[11] L Beirão da Veiga, F Dassi, and A Russo. A $\mathcal{C}^1$ virtual element method on polyhedral meshes. *Computers & Mathematics with Applications*, 79(7):1936–1955, 2020. `doi:10.1016/j.camwa.2019.06.019`.

[12] L Beirão Da Veiga, C Lovadina, and G Vacca. Virtual elements for the Navier–Stokes problem on polygonal meshes. *SIAM Journal on Numerical Analysis*, 56(3):1210–1242, 2018. `doi:10.1137/17m1132811`.

[13] L Beirão da Veiga and G Manzini. A virtual element method with arbitrary regularity. *IMA Journal of Numerical Analysis*, 34(2):759–781, 2014. `doi:10.1093/imanum/drt018`.

[14] L Beirão da Veiga, D Mora, and G Vacca. The Stokes complex for virtual elements with application to Navier–Stokes flows. *Journal of Scientific Computing*, 81:990–1018, 2019. `doi:10.1007/s10915-019-01049-3`.

[15] L Beirão Da Veiga, A Russo, and G Vacca. The virtual element method with curved edges. *ESAIM: Mathematical Modelling and Numerical Analysis*, 53(2):375–404, 2019. `doi:10.1051/m2an/2018052`.

[16] M F Benedetto, S Berrone, S Pieraccini, and S Scialò. The virtual element method for discrete fracture network simulations. *Computer Methods in Applied Mechanics and Engineering*, 280:135–156, 2014. `doi:10.1016/j.cma.2014.07.016`.

[17] S Bertoluzza, M Pennacchio, and D Prada. High order VEM on curved domains. *Rendiconti Lincei*, 30(2):391–412, 2019. `doi:10.4171/rlm/853`.

[18] A Cangiani, E H Georgoulis, T Pryer, and O J Sutton. A posteriori error estimates for the virtual element method. *Numerische mathematik*, 137:857–893, 2017. `doi:10.1007/s00211-017-0891-9`.

[19] F Dassi, A Fumagalli, I Mazzieri, A Scotti, and G Vacca. A virtual element method for the wave equation on curved edges in two dimensions. *Journal of Scientific Computing*, 90:1–25, 2022. `doi:10.1007/s10915-021-01683-w`.

[20] F Dassi, A Fumagalli, A Scotti, and G Vacca. Bend 3d mixed virtual element method for darcy problems. *Computers & Mathematics with Applications*, 119:1–12, 2022. `doi:10.1016/j.camwa.2022.05.023`.

[21] V. Dhanush and S. Natarajan. Implementation of the virtual element method for coupled thermo-elasticity in abaqus. *Numerical Algorithms*, 80(3):1037–1058, 2018. `doi:10.1007/s11075-018-0516-0`.

[22] C M Elliott and T Ranner. Finite element analysis for a coupled bulk–surface partial differential equation. *IMA Journal of Numerical Analysis*, 33(2):377–402, 2013. `doi: 10.1093/imanum/drs022`.

[23] M Frittelli, A Madzvamuse, and I Sgura. Bulk-surface virtual element method for systems of PDEs in two-space dimensions. *Numerische Mathematik*, 147(2):305–348, 2021. `doi: 10.1007/s00211-020-01167-3`.

[24] M Frittelli, A Madzvamuse, and I Sgura. The bulk-surface virtual element method for reaction-diffusion PDEs: analysis and applications. *Communications in Computational Physics*, Accepted, 2023.

[25] M Frittelli, A Madzvamuse, I Sgura, and C Venkataraman. Lumped finite elements for reaction–cross–diffusion systems on stationary surfaces. *Computers & Mathematics with Applications*, 74(12):3008–3023, 2017. `doi:10.1016/j.camwa.2017.07.044`.

[26] M Frittelli, A Madzvamuse, I Sgura, and C Venkataraman. Preserving invariance properties of reaction–diffusion systems on stationary surfaces. *IMA Journal of Numerical Analysis*, 39(1):235–270, 2017. `doi:10.1093/imanum/drx058`.

[27] M Frittelli and I Sgura. Virtual element method for the Laplace-Beltrami equation on surfaces. *ESAIM: Mathematical Modelling and Numerical Analysis*, 52(3):965–993, 2018. `doi:10.1051/m2an/2017040`.

[28] A L Gain, C Talischi, and G H Paulino. On the virtual element method for three-dimensional linear elasticity problems on arbitrary polyhedral meshes. *Computer Methods in Applied Mechanics and Engineering*, 282:132–160, 2014. `doi:10.1016/j.cma.2014.05.005`.

[29] C Herrera, R Corrales-Barquero, J Arroyo-Esquivel, and J G Calvo. A numerical implementation for the high-order 2D virtual element method in MATLAB. *Numerical Algorithms*, 92(3):1707–1721, 2022. `doi:10.1007/s11075-022-01361-4`.

[30] J Huang and S Lin. A posteriori error analysis of a non-consistent virtual element method for reaction diffusion equations. *Applied Mathematics Letters*, 122:107531, 2021. `doi:10.1016/j.aml.2021.107531`.

[31] D Lacitignola, B Bozzini, M Frittelli, and I Sgura. Turing pattern formation on the sphere for a morphochemical reaction-diffusion model for electrodeposition. *Communications in Nonlinear Science and Numerical Simulation*, 48:484–508, 2017. `doi:10.1016/j.cnsns.2017.01.008`.

[32] D Lacitignola, M Frittelli, V Cusimano, and A De Gaetano. Pattern formation on a growing oblate spheroid. an application to adult sea urchin development. *Journal of Computational Dynamics*, 9(2):185–206, 2022. `doi:10.3934/jcd.2021027`.

[33] A Ortiz-Bernardin. Vemlab version 2.4.1. Accessed: 2023-03-07. URL: `https://camlab.cl/software/vemlab/`.

[34] A Ortiz-Bernardin, C Alvarez, N Hitschfeld-Kahler, A Russo, R Silva-Valenzuela, and E Olate-Sanzana. Veamy: an extensible object-oriented C++ library for the virtual element method. *Numerical Algorithms*, 82(4):1189–1220, 2019. `doi:10.1007/s11075-018-00651-0`.

[35] O J Sutton. The virtual element method in 50 lines of MATLAB. *Numerical Algorithms*, 75(4):1141–1159, 2016. `doi:10.1007/s11075-016-0235-3`.

[36] C Talischi, G H Paulino, A Pereira, and I F M Menezes. PolyMesher: a general-purpose mesh generator for polygonal elements written in matlab. *Structural and Multidisciplinary Optimization*, 45(3):309–328, 2012. `doi:10.1007/s00158-011-0706-z`.

[37] G Vacca and L Beirão da Veiga. Virtual element methods for parabolic problems on polygonal meshes. *Numerical Methods for Partial Differential Equations*, 31(6):2110–2134, 2015. `doi: 10.1002/num.21982`.

[38] D van Huyssteen, F L Rivarola, G Etse, and P Steinmann. On mesh refinement procedures for the virtual element method for two-dimensional elastic problems. *Computer Methods in Applied Mechanics and Engineering*, 393:114849, 2022. `doi:10.1016/j.cma.2022.114849`.

[39] L Xiao, M Zhou, and J Zhao. The nonconforming virtual element method for semilinear elliptic problems. *Applied Mathematics and Computation*, 433:127402, 2022. `doi:10.1016/j.amc.2022.127402`.

[40] J Zhao, B Zhang, and X Zhu. The nonconforming virtual element method for parabolic problems. *Applied Numerical Mathematics*, 143:97–111, 2019. `doi:10.1016/j.apnum.2019.04.002`.